The Pennsylvania State University
The Graduate School

DATA-DRIVEN STATE OF HEALTH ESTIMATION IN SPARSELY SAMPLED LEAD-ACID BATTERY PACKS

A Thesis in
Mechanical Engineering
by
Gabriel J Worman

© 2023 Gabriel J Worman

Submitted in Partial Fulfillment
of the Requirements
for the Degree of

Master of Science

May 2023

The thesis of Gabriel J Worman was reviewed and approved by the following:

Christopher D. Rahn
Professor of Mechanical Engineering
Thesis Advisor

Jared Butler
Assisstant Professor of Mechanical Engineering

Robert Kunz
Professor of Mechanical Engineering
Department Head of Mechanical Engineering

Abstract

Batteries degrade over time, so estimating their state of health (SoH) is critical to proper functioning of battery packs. Electric vehicles (EVs) in particular, can stall if the battery pack does not provide sufficient voltage to operate the electric motors (Vmin). The battery voltage depends on its state of charge (SoC), capacity (Q), internal resistance (IR), and discharge current (I). SoC and I are dynamic functions of time that vary during driving. Q and IR slowly change over time due to cell temperature and aging. In this work, three parameters associated with battery SoH are estimated from EV lab and field data, Q, IR, and cyclic Vmin. The data are collected from golf cars powered by six 8 V valve regulated lead-acid absorbent glass mat batteries. One EV is tested in a lab environment and the others are in use at a golf course. Data are sampled every five minutes for eight months and include max, min, average and instantaneous voltage and current, integrated current, and temperature. Q is estimated using discharge SoC and current throughput. IR is estimated using voltage and current during charging and compensated for temperature variations. Finally, the cyclic minimum voltage is tracked. The field and lab test data show aging trends for each of the three SoH parameters. Linear approximations are applied to these trends, with low mean absolute errors (MAE) seen for all batteries. Average MAE for Q is 11.83 Ah, with a standard deviation of 2.56 Ah. Average MAE for Vmin is 0.14 V, with a standard deviation of 0.064 V. Average MAE for IR is 3.31 mΩ with a standard deviation of 0.73 mΩ. The lab data show similar trends, but with much smaller MAE.

Table of Contents

List of Figures

List of Tables

List of Abbreviations and Symbols

Acronyms and Abbreviations

AGM	Absorbent Glass Mat
DoD	Depth of Discharge
IoT	Internet of Things
IR	Internal Resistance
MAE	Mean Absolute Error
OCV	Open Circuit Voltage
Q	Capacity
SoC	State of Charge
SoH	State of Health
VRLA	Valve Regulated Lead-Acid
Vmin	Cyclic Minimum Voltage

Symbols

I	Current
I_{max}	Maximum Current
I_{min}	Minimum Current
V_{min}	Minimum Voltage
V_{max}	Maximum Voltage
$\hat{Q}$	Capacity Estimate
$\hat{R}$	Internal Resistance Estimate
$\hat{SoC}$	State of Charge Estimate

Chapter 1
Introduction

1.1 Background

Batteries degrade over time, so estimating their state of health (SoH) is critical to proper functioning of battery packs. Many efforts to understand and track aging in batteries has been performed over the years ranging from simple approaches to more complex ones.

Sun et al., 2011 developed a voltage measurement based approach to estimate SoH in lead-acid batteries [1]. Saha et al., 2007 used Bayesian estimation in their SoH estimation [2]. Khodadadi et al., 2021 developed a physics-based model to estimate SoH [3].

Previous research on SoH estimation assumed that high fidelity and high sample rate data was available in real-time. This required a large amount of data storage and processing power on the vehicle which added cost and complexity to the battery management system. An alternative approach is to collect the data, compress the data, and transmit the data to the cloud where it can be stored and processed.

1.2 Research Scope

This work studies aging in valve regulated lead-acid (VRLA) absorbent glass mat (AGM) batteries. This is done by defining, estimating, and tracking three parameters related to SoH: capacity (Q), internal resistance (IR), and cyclic minimum voltage (Vmin). The sparsely sampled data includes the instantaneous voltage, current, and temperature and derived/compressed data from averaging, integrating, max/min of the data during the five minute sample period.

The batteries are placed in golf cars as the primary energy source for their motive needs, with the cars being in near daily use. That use is not controlled and purely emerges from the day-to-day needs of the golf course and golfers. Typically, the cars are charged overnight to a full charge and then used throughout the day. The usage has variation between each car and from day to day. Two additional battery strings are run in the lab with simulated and unchanging loads.

The focus of this work is to track aging in real-world EV applications with compressed and sparsely

Table 1.1. Measured and Calculated Data

Value	Unit	Method[a]	Timing[b]	Granularity[c]
Time	sec	M	I	S
Voltage	V	M	I	B
Current	A	M	M	S
Temperature	C	M	I	S
State[d]	N/A	B	I	S
Current Thoughput	Ah	C	I	S
Max Voltage	V	C	A	B
Min Voltage	V	C	A	B
Max Current[e]	A	C	A	S
Min Current[f]	A	C	A	S

[a]M: Measured onboard, C: Calculated onboard, B: BMS controlled
[b]I: Instantaneous, M: Mean, A: Asynchronous
[c]B: Individual battery, S: String
[d]System state: discharge, bulk charge, float charge, or idle
[e]Current at Vmax
[f]Current at Vmin

sampled data where usage conditions continuously change. The data span eight months, so temperature trends over the seasons are observed. Internal resistance is especially sensitive to temperature [4,5], so this effect is included to isolate aging/SoH.

1.3 Sparsely Sampled Data

The data from the golf cars are streamed to the cloud via an internet of things (IoT) device. Data are reported with a sampling time of 300 seconds to minimize the data that are transmitted. This sparse sampling creates a need for data compression techniques that assist SoH estimation. The wireless transmission of data can be intermittent, sometimes resulting in a sampling time of 600 seconds or longer.

Each golf car has six, 8 V batteries connected in series to produce 48 V. Table 1.1 shows the measured and calculated data transmitted by each vehicle. Voltage is measured at the terminal of each battery at 2000 Hz. The batteries are in series, so the current for the string (and every battery) is measured with one sensor. A single temperature sensor provides temperature measurements for the string. The real-time IoT data sampled at high frequency are transmitted to the cloud every five minutes. The voltage and temperature are the measured values at the instant of sampling and the current is the average value over the sample period.

Additional data is provided at each sample time with compressed information about measured values during the sample period. Current throughput is calculated by current integration. The minimum and maximum string voltages and associated currents are also reported.

The onboard state variable indicates whether the battery is in charge, idle, or discharge mode. The charge portion of the cycle is further split into bulk and float charging modes. During a normal cycle, the golf cars are typically plugged in to charge in the late evening and left to charge through the night. Once a full charge is reached, charging stops and the batteries remain in an idle state until the golf car is used. The car is then used throughout the day. In practice, a second charging period during the middle of the day is sometimes seen. Incomplete charging and/or skipping the idle portion can also happen.

In addition to the nine golf cars in daily use, two battery strings are tested in the laboratory. The same measurements and calculated values are reported at 300 second sampling. The batteries are charged with the same chargers provided with a defined load cycle.

Figure 1.1 shows a typical day for one battery in one of the field-tested golf cars. The car is fully charged at t=0 hrs (morning). The battery voltage is high 8.56 V and temperature is low 26.8°C. It goes out on the course for some rounds of golf. The battery voltage drops to 8.25 V as the current throughput increases to 54.2 Ah. The nameplate capacity of the cell is 130 Ah, so this corresponds to a SoC of 58.3%. At the end of the day, it is put on charge. The current immediately jumps to a high, positive value and the voltage and Ah increase. Charge completes during the middle of the night and the state switches to idle until morning.

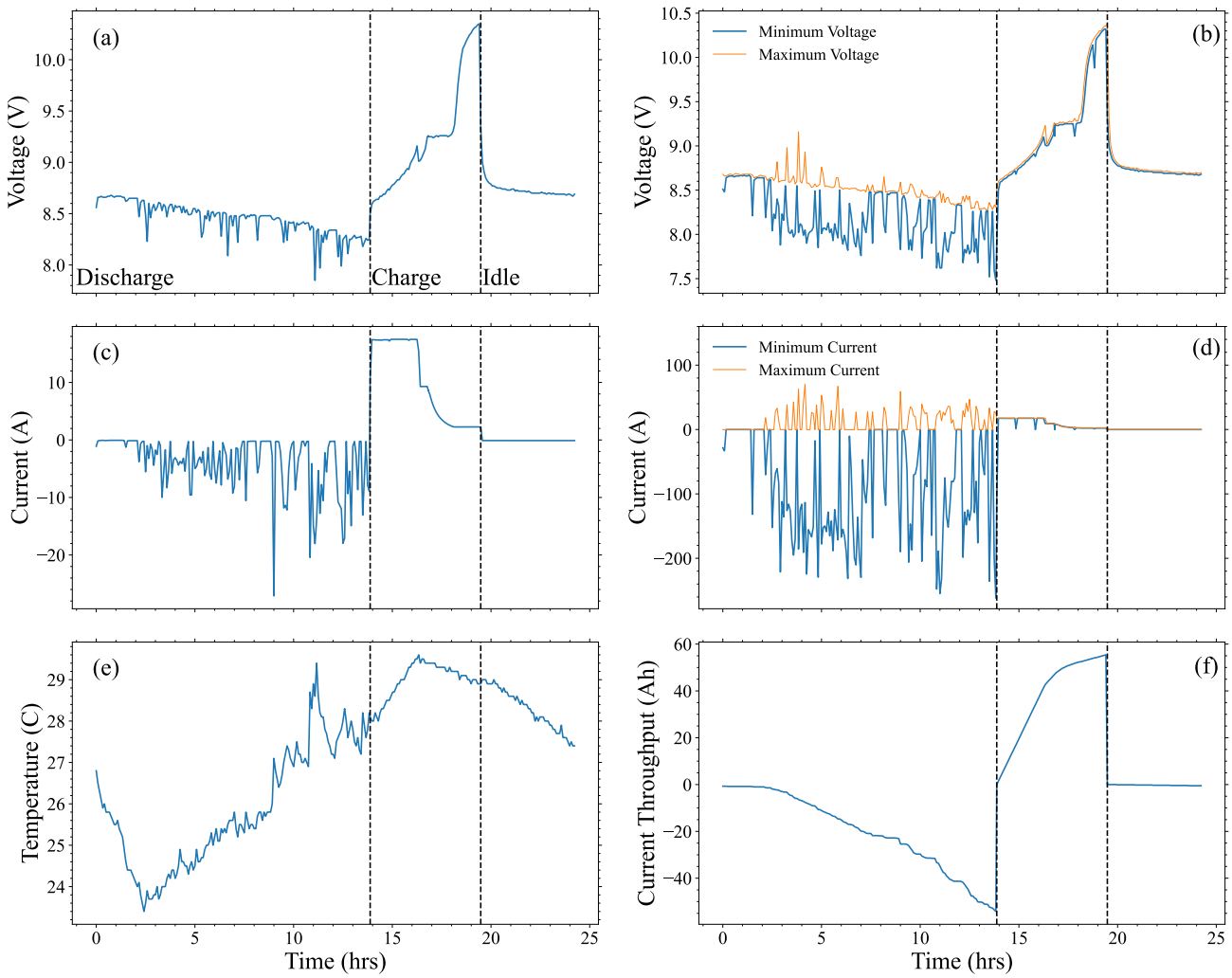

Figure 1.1. Battery data for a typical day from a field-tested golf car: (a) Instantaneous voltage, (b) V_{min} and V_{max}, (c) $\bar{I}$, (d) I_{min} and I_{max}, (e) Temperature (f) Integrated I which is reset to 0 Ah at each each battery mode: discharge, charge, and idle.

Chapter 2
Battery State Estimation from Sparsely Sampled Data

2.1 State of Charge Estimation

State of Charge (SoC), is a measure of usable battery capacity:

$$SoC(t) = \frac{Q + \int_0^t I\,dt}{Q} = 1 - DoD(t), \tag{2.1}$$

where Q is the battery capacity in amp-hours (Ah), $I(t)$ is the current (>0 for charging), and DoD is depth of discharge. A fully charged battery has 100% SoC and fully discharged has 0% SoC [6].

SoC can be estimated from the measured voltage. If the battery is maintained at zero current for a long time, the open-circuit voltage (OCV) is related to SoC with an empirical OCV curve. If the current is nonzero, however, estimating SoC from the inverse of the OCV curve becomes less accurate. One can improve the SoC estimation by using OCV curves that depend on current.

Figure 2.1 shows the relationship between SoC and OCV for a C-rate of C/3 (C-rate is the function of capacity discharged or charged in one hour [7]). The C/3 rate is used to determine SoC because it matches the typical discharge rate of the cars.

A quadratic curve fit is used to estimate SoC

$$\hat{SoC} = 0.1623(OCV)^2 - 1.309(OCV) + 0.2929 \tag{2.2}$$

The $\hat{SoC}$ is limited to 100% to eliminate the effects of overcharge when some current produces water loss without increasing stored energy.

The battery packs are in near constant use, so they do not achieve an open circuit condition, which can

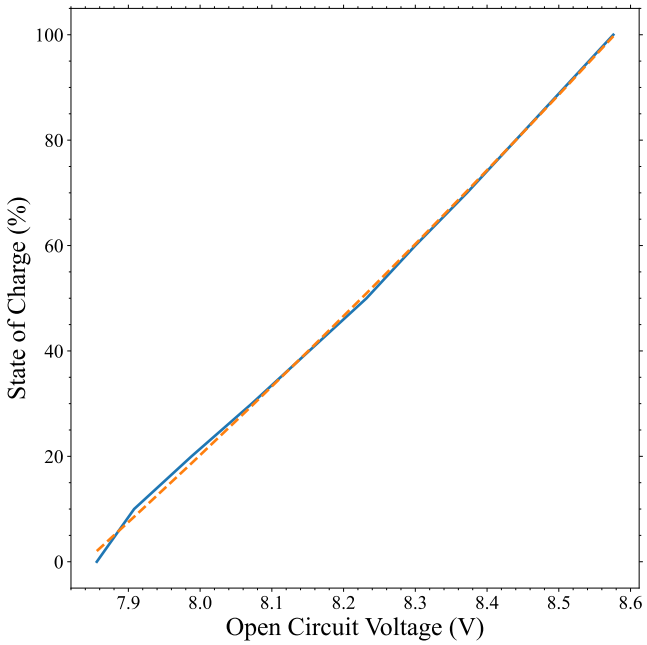

Figure 2.1. SoC versus OCV data (solid) and curve fit (dashed).

require more than a day [6]. Rest periods are identified during the day when

$$| \overline{I_k} | < \frac{Q}{200} \quad | I_{max_k} | < \frac{Q}{100} \quad | I_{min_k} | < \frac{Q}{100} \tag{2.3}$$

corresponding to periods when the average, max, and min current are very small during the sample period.

Figure 2.2 shows the $\hat{SoC}$ estimation results for a typical day. $\hat{SoC}$ is estimated from measured voltage during periods of rest based on Eq. (2.3).

The $\hat{SoC}$ estimates generally track the current integration results for Q = 133 Ah. Thus, if capacity is known, the current integration provides another $\hat{SoC}$ estimate. OCV based $\hat{SoC}$ estimation during quiet periods, however, can remove bias/drift/overcharge effects.

2.2 Capacity Estimation

Battery capacity (Ah) is defined as the total charge that can be discharged from 100% SoC to 0% SoC under ideal conditions (room temperature and low C-rate). This differs from the amount of charge that can actually be discharged in the field. The battery manufacturer provides a name-plate capacity but this may only be accurate during part of the battery's life. Many methods have been developed to estimate this important aging metric [8–10].

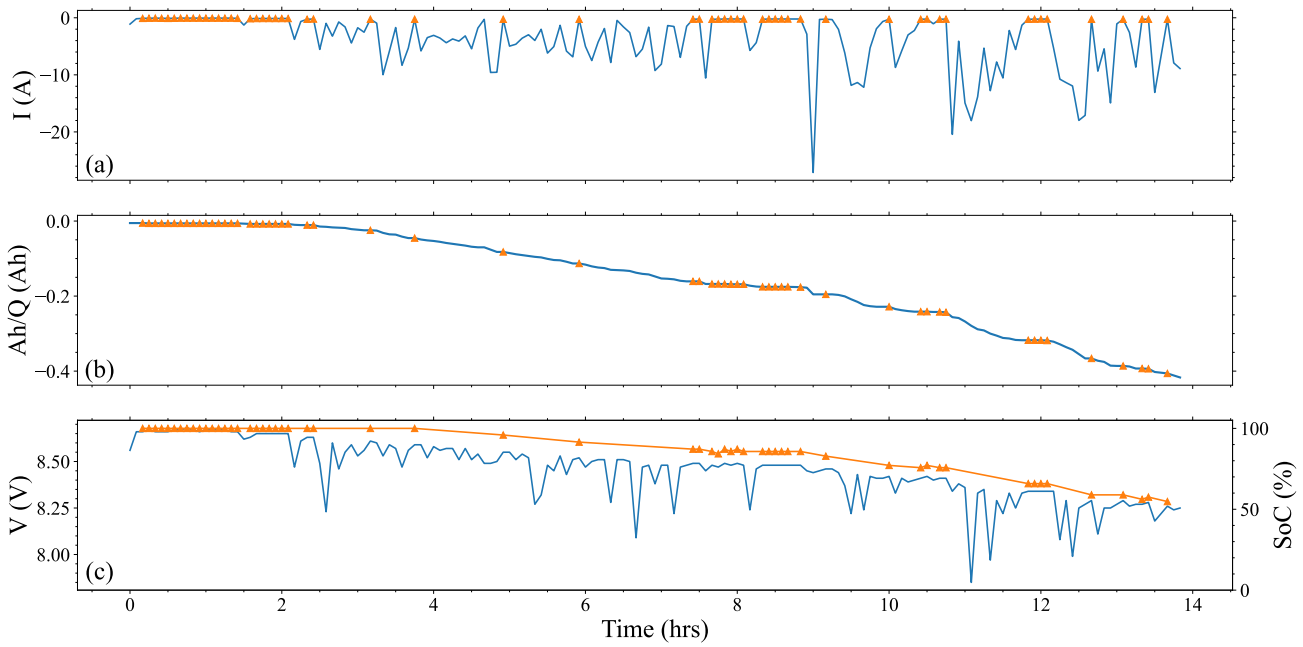

Figure 2.2. $\hat{SoC}$ estimation from voltage after rest periods (△): (a) Current, (b) Current integration, and (c) Voltage and $\hat{SoC}$ estimate.

In this work, SoC and current during discharge estimate capacity

$$\hat{Q} = \frac{\int_{t_1}^{t_2} I\,dt}{SoC(t_2) - SoC(t_1)}, \tag{2.4}$$

where t_1 and t_2 are two quiescent times during a discharge cycle. In practice, a point at the beginning of discharge and a point near the end are used. This gives a large change in SoC (and denominator in Eq. (2.4)) to minimize noise in $\hat{Q}$. Using quiescent data according to inequality (2.2) ensures that $\hat{SoC}$ estimation is accurate.

Figure 2.3 shows the SoC and current throughput for a typical discharge cycle for a single battery. The capacity estimate

$$\hat{Q} = \frac{\Delta Ah}{\Delta SoC}, \tag{2.5}$$

where $\Delta Ah = Ah_1 - Ah_2$ and $\Delta SoC = SoC_1 - SoC_2$. In this example, $\hat{Q}$ = 116.7 Ah. Thresholds help mitigate estimation noise. A minimum value of 10 Ah for ΔAh is required to compute $\hat{Q}$. The SoC change must be > 1%.

Figures 2.4 and 2.5 show the $\hat{Q}$ results for an example string in the field and lab, respectively. Capacity is estimated and a best fit line found for each of the 54 field-batteries and 6 lab batteries. Mean absolute error:

$$MAE = \frac{\sum |y_{predicted} - y_{true}|}{n}, \tag{2.6}$$

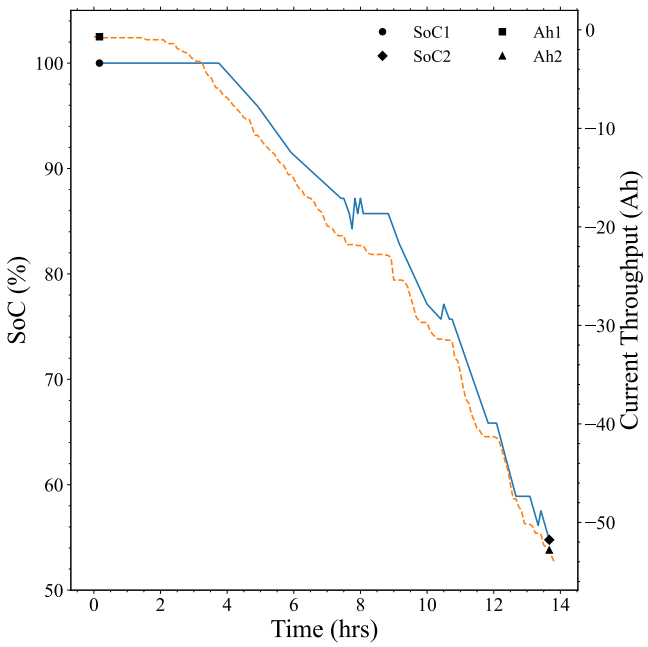

Figure 2.3. Example capacity results for a discharge cycle, SoC (solid), current throughput (dashed).

is used to represent the error in the linear fits for the trends seen in $\hat{Q}$. The average MAE for $\hat{Q}$ is 11.83 Ah with a standard deviation of 2.56 Ah. The lab data average MAE is 0.43 Ah with a standard deviation of 1.22 Ah.

Typical values for $\hat{Q}$ in the field data match closely with the name-plate capacity while the lab results are lower. The lab data show less noise due to the repeated discharge cycle. Trends in $\hat{Q}$ are clear and predictable.

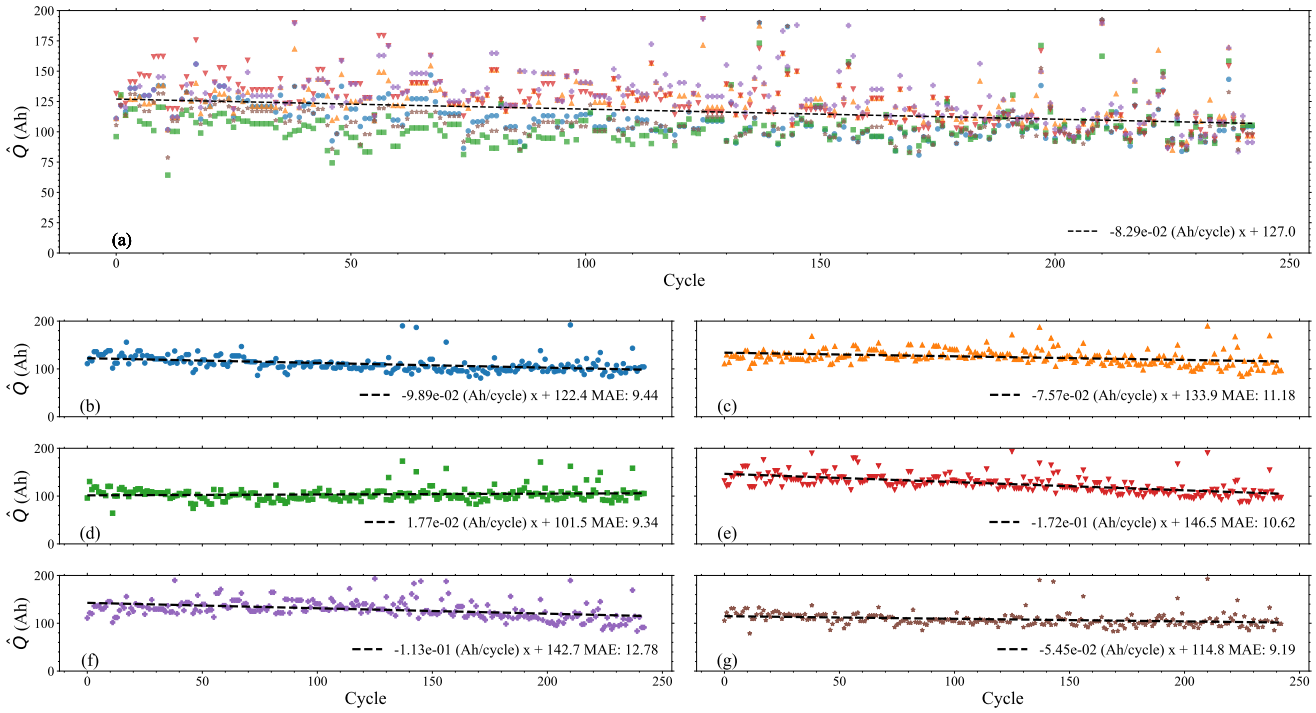

Figure 2.4. Capacity estimation results (•) and best fit trendlines from field data for (a) String, (b) Battery #1, (c) Battery #2, (d) Battery #3, (e) Battery #4, (f) Battery #5, (g) Battery #6.

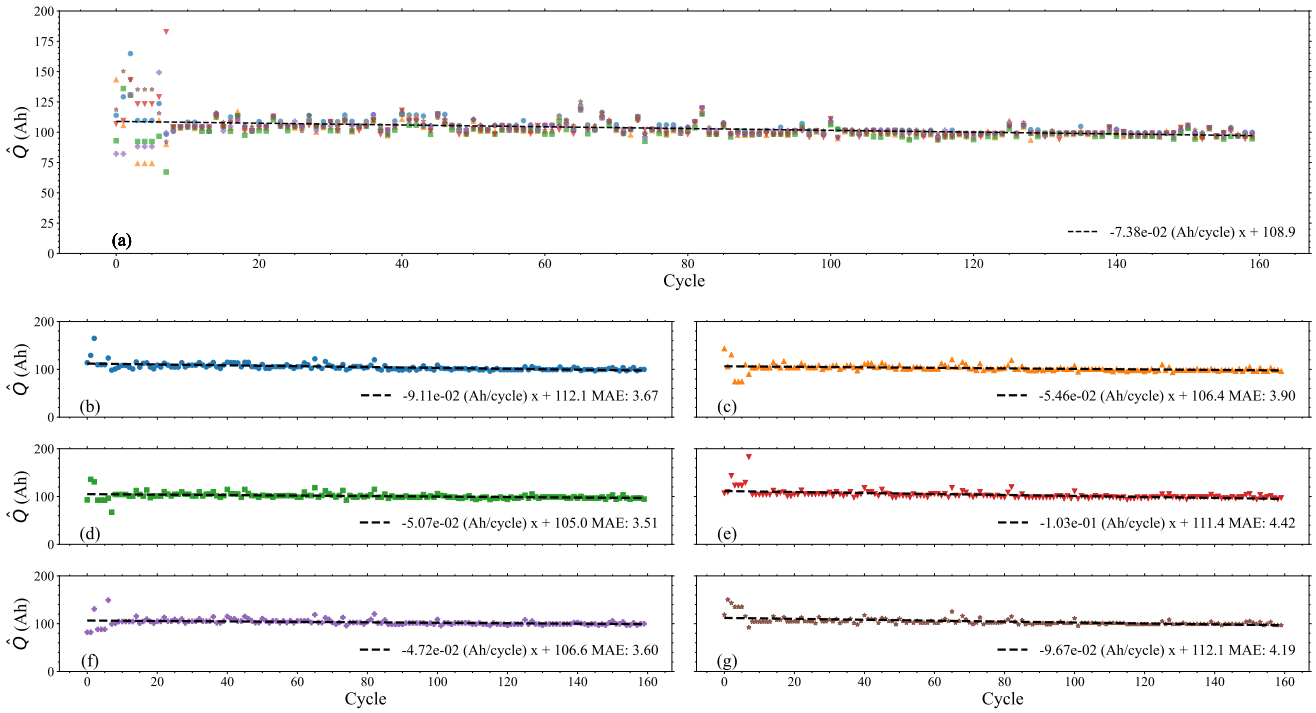

Figure 2.5. Capacity estimation results (•) and best fit trendlines from lab data for (a) String, (b) Battery #1, (c) Battery #2, (d) Battery #3, (e) Battery #4, (f) Battery #5, (g) Battery #6.

2.3 Internal Resistance

Equivalent series resistance or internal resistance (IR) [2, 11] is governed by Ohm's Law

$$\Delta V = \Delta I R. \tag{2.7}$$

Eq. (2.7) can be used when a battery experiences a step change in current (ΔI) causing a step change in voltage (ΔV). The CCCV charging process provides opportunities with large ΔI (e.g., start of charge) that produces large ΔV and accurate $\hat{R}$ according to Eq. (2.7).

Figure 2.6 shows the (CC1-CC2-CV-CC3) charge cycle used by the golf car chargers, CC1 of 17.5 A and is followed by CC2 of 9.3 A, CV, and CC3 of 2 A. The CC phases end when voltage reaches a threshold. CV phase ends when current crosses a threshold.

The switch from CC1 to CC2 is used to estimate IR,

$$\hat{R} = \frac{\Delta V}{8.2A} \tag{2.8}$$

where ΔV is the change in voltage at the switch and ΔI is the change in current at the switch from CC1 to CC2. The voltage change is the difference between the max and min voltage values during the sampling period where the switch from CC1 to CC2 occurs. At the switch from 17.5 A to 9.3 A, the max voltage occurs immediately before the switch and the minimum voltage occurs just after the switch. Figure 2.6 shows an example result for a single battery from the field data where $\hat{R}$ = 25.6 mΩ, in the observed range of 20 to 50 mΩ of all the batteries.

Temperature affects the speed of the chemical reactions and electronic resistances within the battery [4, 5, 12]. Thus, it is important to filter the effect of temperature changes on $\hat{R}$ to more accurately track the impedance rise due to aging. The field data spans eight months and the temperature varied from roughly 10°C to 40°C with some days below 0°C at the golf course in Texas where the data were collected.

Figure 2.7 shows the best fit line of the $\hat{R}$ and temperature for an example battery

$$\hat{R} = bT(^\circ C) + c \tag{2.9}$$

with average values over 54 batteries of b = -0.653 and c = 46.7. $\hat{R}$ is then temperature compensated

$$\hat{R}_t = \hat{R} - b(T - 25^\circ C) \tag{2.10}$$

where $\hat{R}_t$(25°C) = $\hat{R}$. The linear fit is best above 15°C for this battery as $\hat{R}$ estimates below this temperature fall outside the linear approximation.

Figures 2.8 shows $\hat{R}$ versus time for an example battery in field testing. The temperature compensated

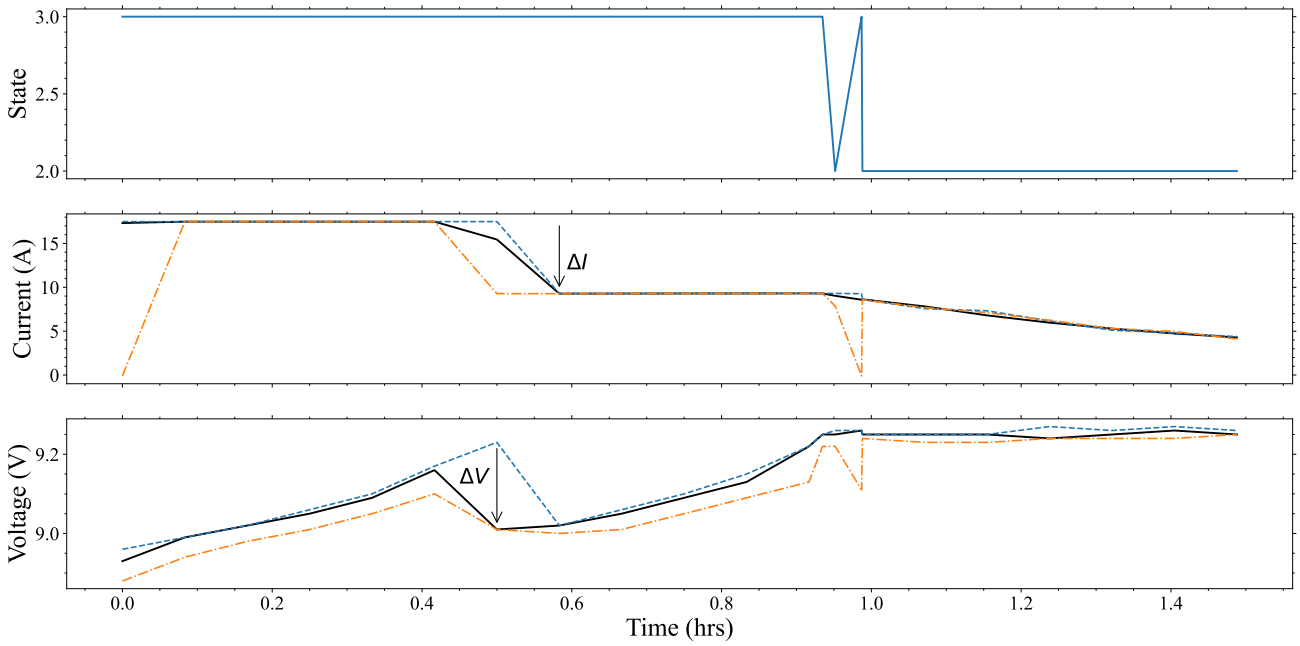

Figure 2.6. IR estimation at the CC1 to CC2 switch: (a) State, (b) $\bar{I}$ (solid), I_{max} (dashed), I_{min} (dot dashed), (c) V (solid), V_{max} (dashed), V_{min} (dot dashed).

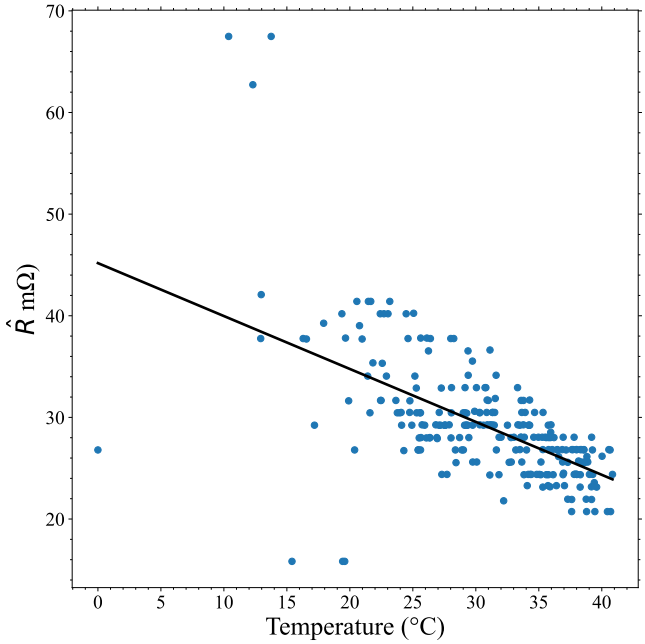

Figure 2.7. $\hat{R}$ estimate versus temperature with best fit line $\hat{R}$ = -0.52T + 45.18.

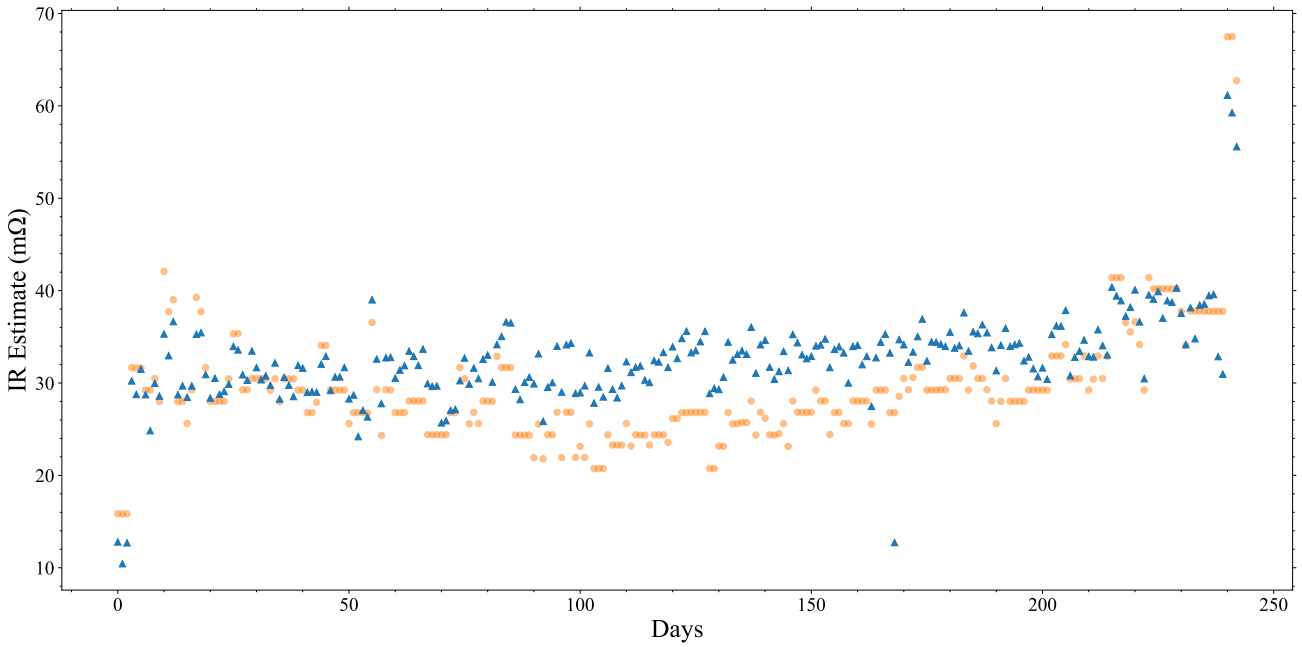

Figure 2.8. IR estimates for field test data without ($\hat{R}$, •) and with ($\hat{R}_t$, △) temperature compensation.

$\hat{R}_t$ is generally above $\hat{R}$, indicating warmer than 25°C temperature at this course. The $\hat{R}_t$ results have a generally increasing trend as expected with calendar/usage aging.

Figures 2.9 and 2.10 show the $\hat{R}_t$ results for an example string in the field and lab, respectively. $\hat{R}_t$ again increases monotonically. The best fit lines of the field and lab data show positive slopes. Average MAE seen in the field data is 3.31 $m\Omega$ with a standard deviation of 0.73 $m\Omega$. Again, the lab results show smaller error with average MAE being 0.31 $m\Omega$ and a standard deviation of 0.96 $m\Omega$.

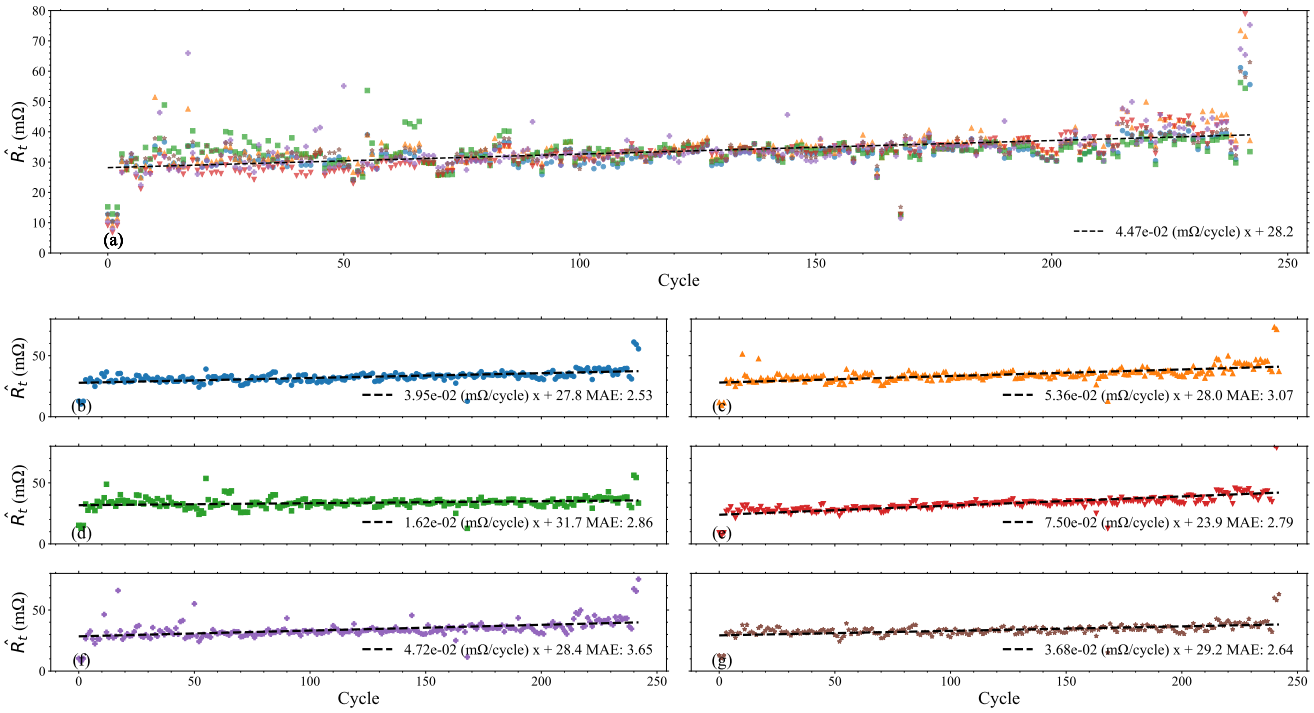

Figure 2.9. Internal resistance estimation results (•) and best fit trendlines from field data for (a) String, (b) Battery #1, (c) Battery #2, (d) Battery #3, (e) Battery #4, (f) Battery #5, (g) Battery #6.

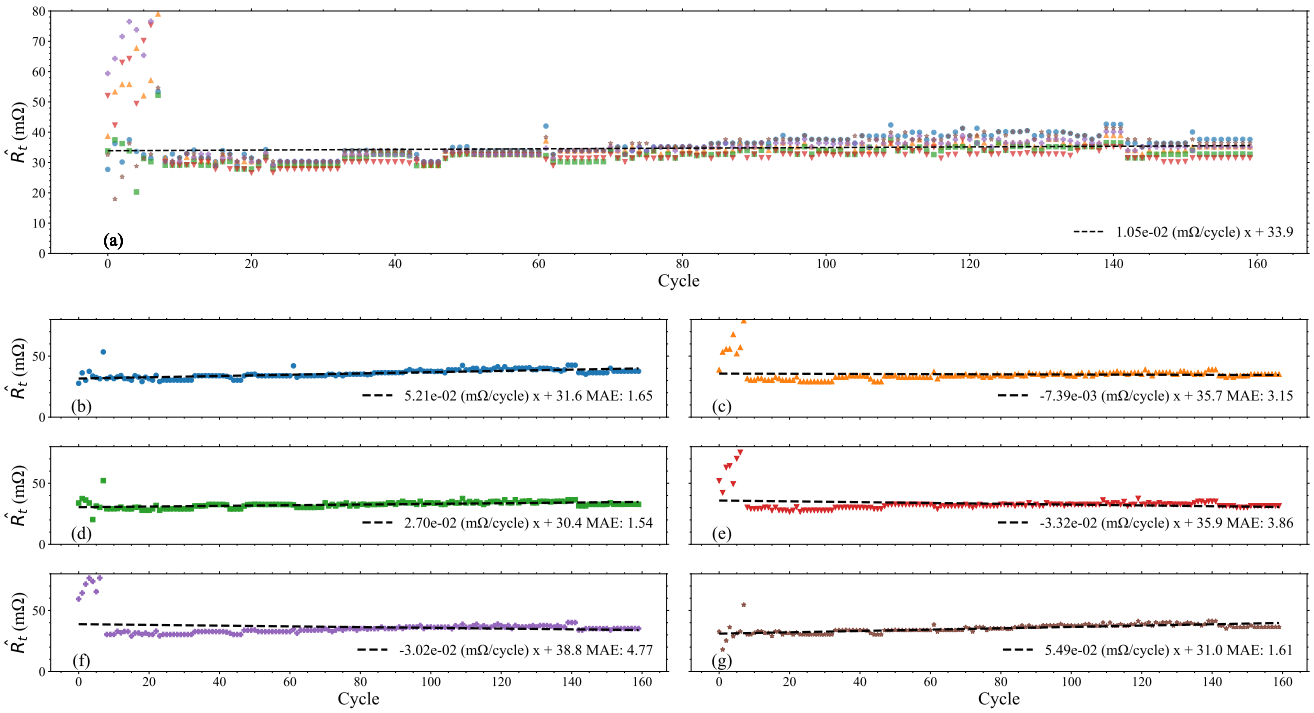

Figure 2.10. Internal resistance estimation results (•) and best fit trendlines from lab data for (a) String, (b) Battery #1, (c) Battery #2, (d) Battery #3, (e) Battery #4, (f) Battery #5, (g) Battery #6.

2.4 Cyclic Minimum Voltage

Figures 2.12 and 2.13 show the Vmin results for an example string in the field and lab, respectively. The best fit lines to the field and lab data show negative trends. The average MAE for the field data is 0.14 V with a standard deviation of 0.064 V. The MAE for the lab data is 0.0039 V with a standard deviation of 0.011 V. Generally, the individual cell Vmin data closely tracks the string data.

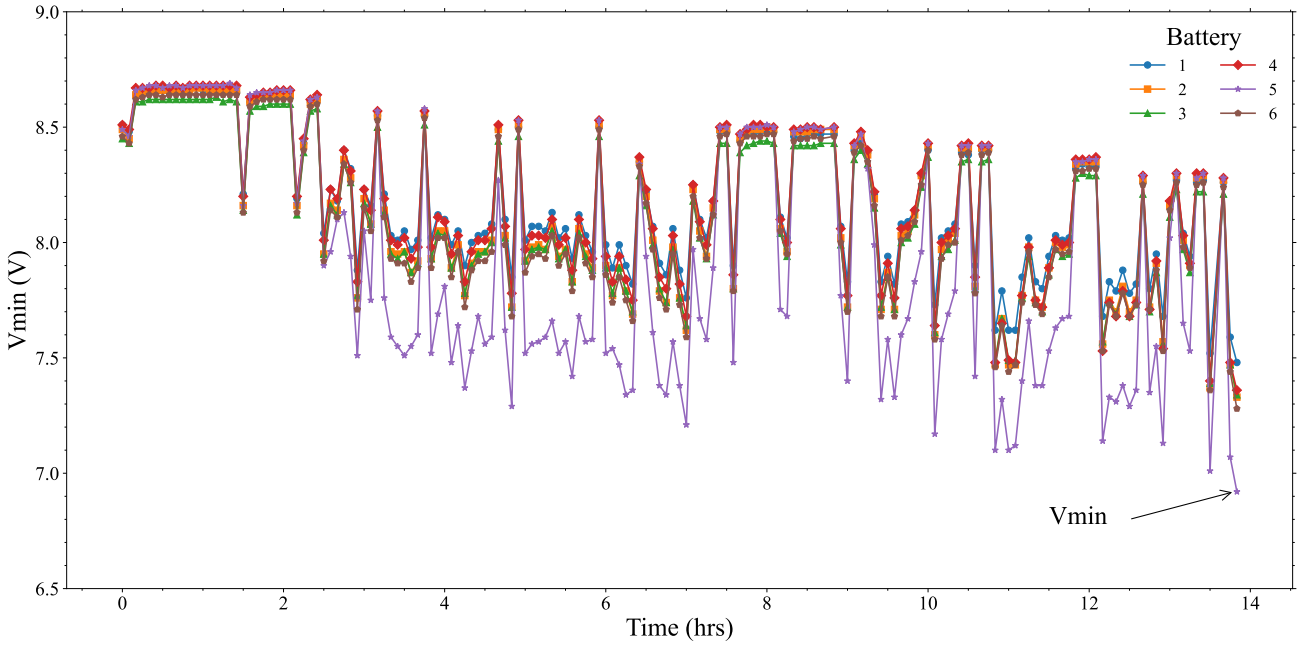

Figure 2.11. Example Vmin of all batteries in a string during a discharge cycle.

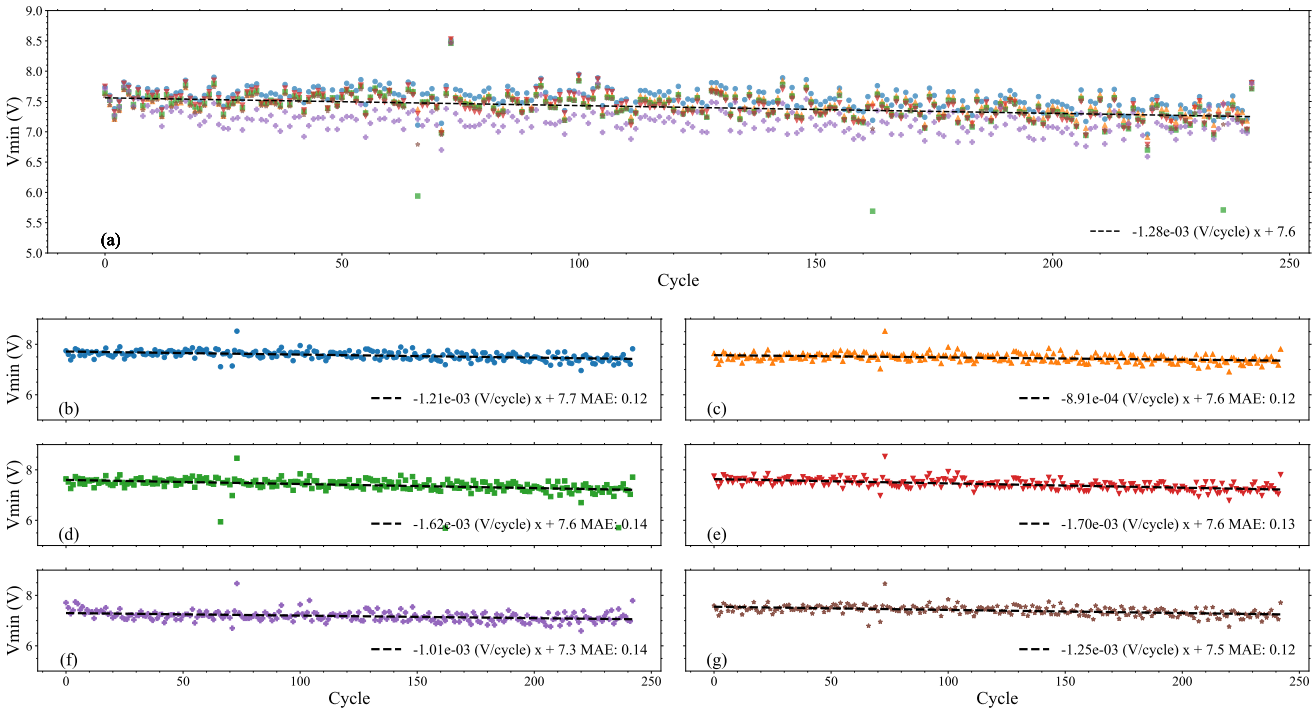

Figure 2.12. Vmin estimation results (•) and best fit trendlines from field data for (a) String, (b) Battery #1, (c) Battery #2, (d) Battery #3, (e) Battery #4, (f) Battery #5, (g) Battery #6.

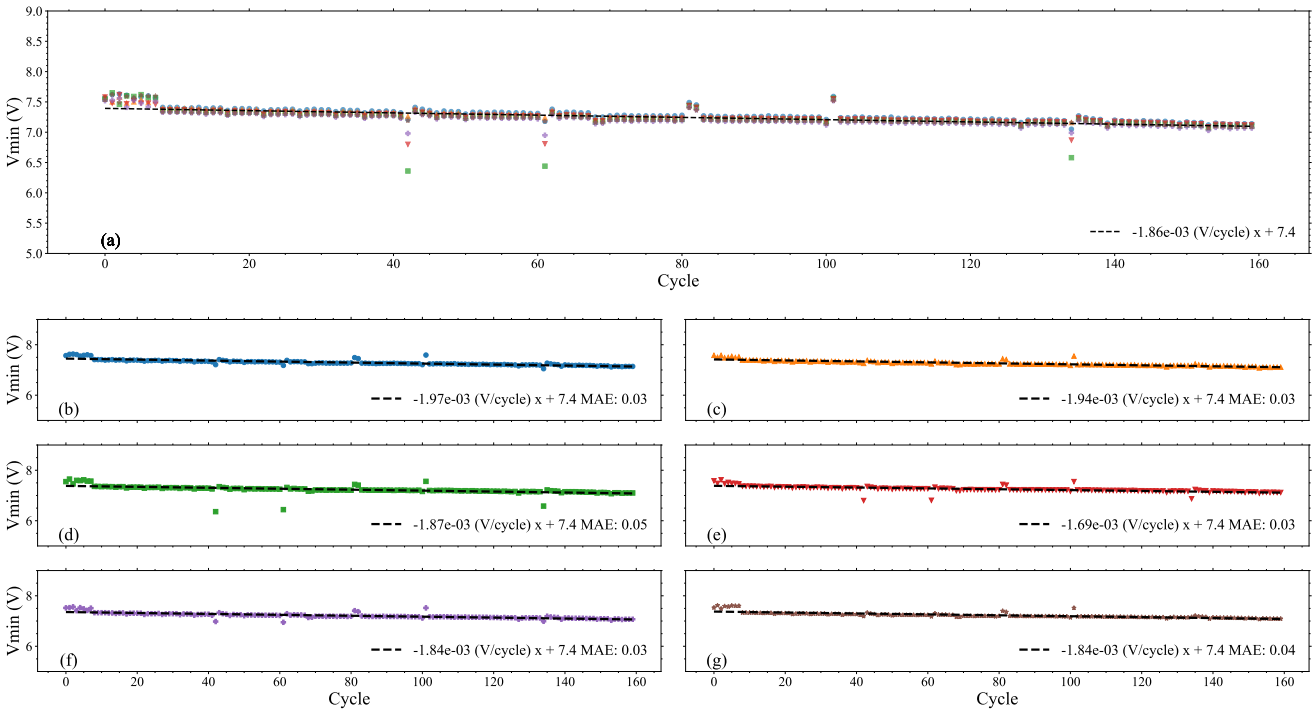

Figure 2.13. Vmin estimation results (•) and best fit trendlines from lab data for (a) String, (b) Battery #1, (c) Battery #2, (d) Battery #3, (e) Battery #4, (f) Battery #5, (g) Battery #6.

Chapter 3
Conclusions

SoH estimates of batteries can be obtained from sparsely sampled voltage, current, and temperature data using compressed (max, min, and average) information. In this work, the field test data show aging trends for each of the three SoH parameters. Linear approximations are applied to these trends, with low mean absolute errors (MAE) seen for all 54 field batteries. Average MAE for Q is 11.83 Ah, with a standard deviation of 2.56 Ah. Average MAE for Vmin is 0.14 V, with a standard deviation of 0.064 V. Average MAE for IR is 3.31 mΩ with a standard deviation of 0.73 mΩ. The lab data show similar trends, but with much smaller MAE.

Bibliography

[1] SUN, Y.-H., H.-L. JOU, and J.-C. WU (2011) "Aging estimation method for lead-acid battery," *IEEE Transactions on Energy Conversion*, **26**(1), p. 264–271.

[2] SAHA, B., S. POLL, K. GOEBEL, and J. CHRISTOPHERSEN (2007) "An integrated approach to battery health monitoring using bayesian regression and state estimation," *2007 IEEE Autotestcon*.

[3] KHODADADI SADABADI, K., P. RAMESH, P. TULPULE, Y. GUEZENNEC, and G. RIZZONI (2021) "Model-based state of health estimation of a lead-acid battery using step-response and emulated in-situ vehicle data," *Journal of Energy Storage*, **36**, p. 102353.

[4] KRIVIK, P., P. BACA, and J. KAZELLE (2020) "Influence of temperature on impedance changes of lead-acid battery cell," *ECS Transactions*, **99**(1), p. 105–115.

[5] BRODA, B. and G. INZELT (2018) "Internal resistance and temperature change during over-discharge of lead-acid battery," *Journal of Electrochemical Science and Engineering*.

[6] PETROVIC, S. (2021) *Battery technology crash course: A concise introduction*, Springer.

[7] CADIRCI, Y. and Y. OZKAZANC (2004) "Microcontroller-based on-line state-of-charge estimator for sealed lead–acid batteries," *Journal of Power Sources*, **129**(2), p. 330–342.

[8] HE, Q., Y. ZHA, Q. SUN, Z. PAN, and T. LIU (2017) "Capacity fast prediction and residual useful life estimation of valve regulated lead acid battery," *Mathematical Problems in Engineering*, **2017**, p. 1–9.

[9] SHEN, W. (2007) "State of available capacity estimation for lead-acid batteries in electric vehicles using neural network," *Energy Conversion and Management*, **48**(2), p. 433–442.

[10] YANG, S.-K. and C.-Y. HUANG (2014) "Residual capacity estimation for lead–acid batteries used in automobiles by the method of median internal resistance," *Journal of Failure Analysis and Prevention*, **14**(3), p. 412–419.

[11] VACCARO, F. J. and P. CASSON (1987) "Internal resistance: Harbinger of capacity loss in starved electrolyte sealed lead acid batteries," *INTELEC '87 - The Ninth International Telecommunications Energy Conference*.

[12] COLEMAN, M., C. ZHU, C. LEE, and W. HURLEY (2005) "A combined SOC estimation method under varied ambient temperature for a lead-acid battery," *Twentieth Annual IEEE Applied Power Electronics Conference and Exposition, 2005. APEC 2005.*